Supporting Information

Insoluble Small-Molecule Organic Cathodes for Highly Efficient Pure Organic Li-Ion Batteries

Xinxin Wang[a], Wu Tang[a], Yang Hu[a], Wenqiang Liu[a], Yichao Yan[b], Liang Xu[c] and Cong Fan[*a]

a. School of Materials and Energy, University of Electronic Science and Technology of China (UESTC), Chengdu 611731, P. R. China

b. State Key Laboratory of Electronic Thin Films and Integrated Devices, University of Electronic Science and Technology of China (UESTC), Chengdu 611731, P. R. China

c. Department of Chemistry and Key Laboratory for Preparation and Application of Ordered Structural Materials of Guangdong Province, Shantou University, Shantou 515063, P. R. China

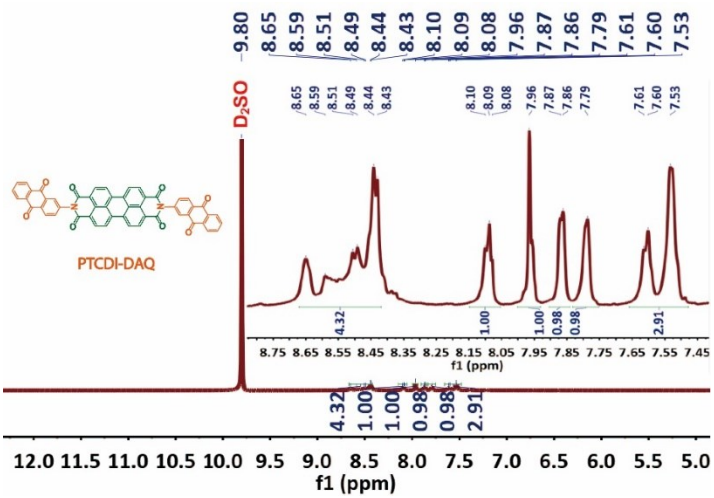

Figure S1. ^{1}H NMR spectrum of PTCDI-DAQ.

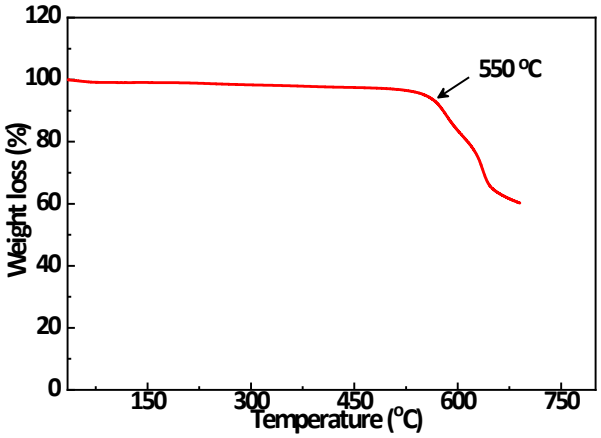

Figure S2. TGA analysis of PTCDI-DAQ.

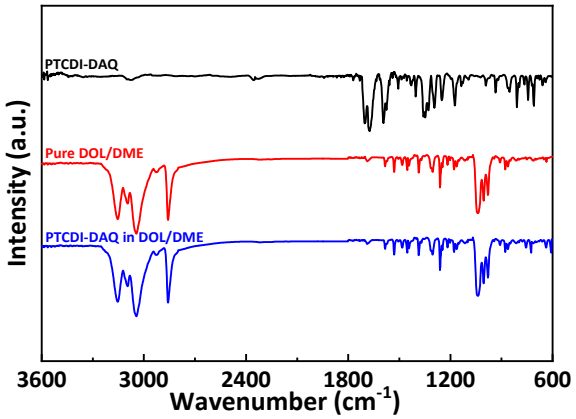

Figure S3. FT-IR spectroscopy of PTCDI-DAQ powder, pure DOL/DME and soaked DOL/DME (immersing PTCDI-DAQ powder into DOL/DME for 7 days), respectively.

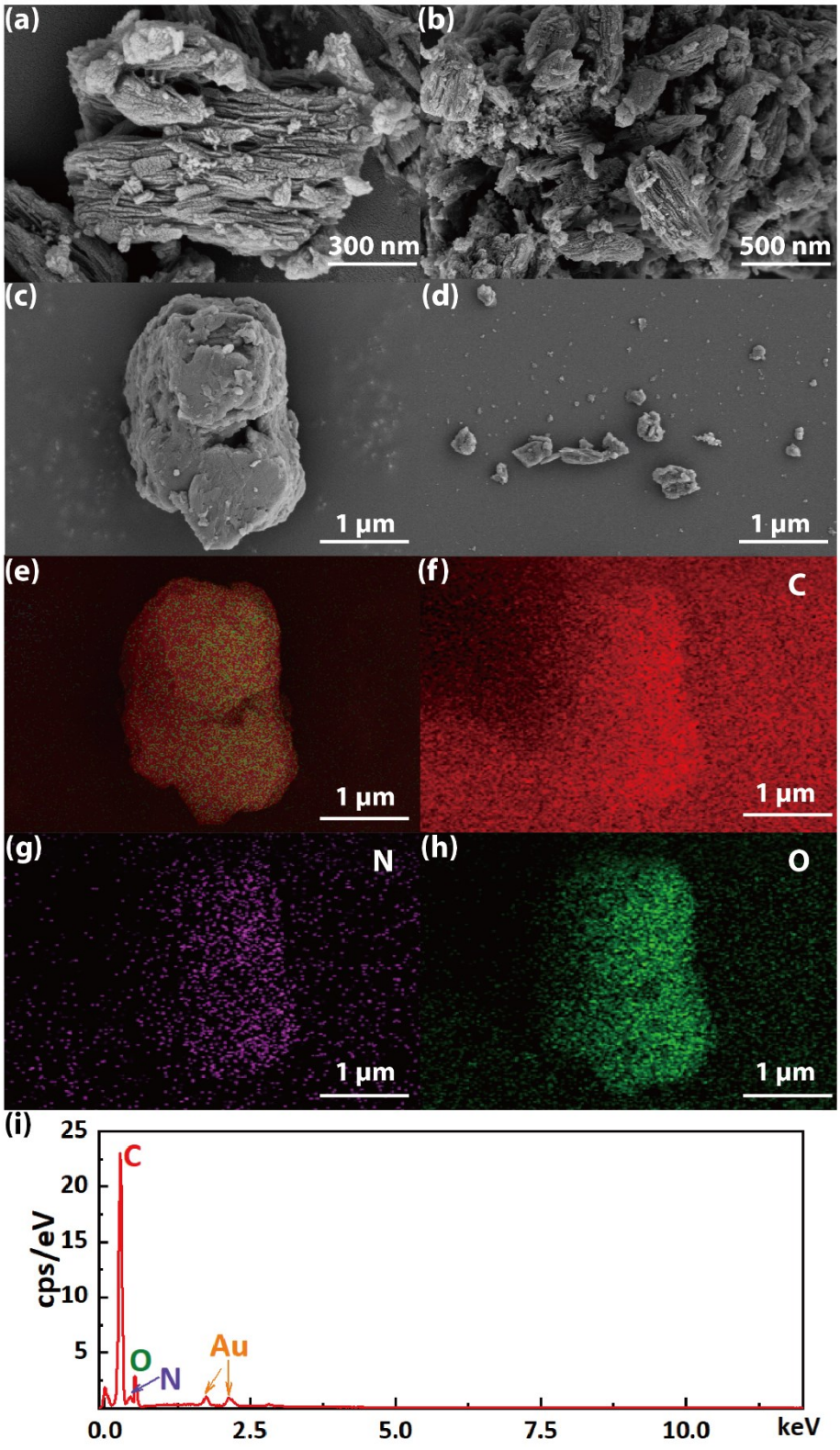

Figure S4. The (a-d) SEM images, (e-h) mapping and (i) energy dispersive spectrometer (EDS) images of C, N, O elements for pure PTCDI-DAQ.

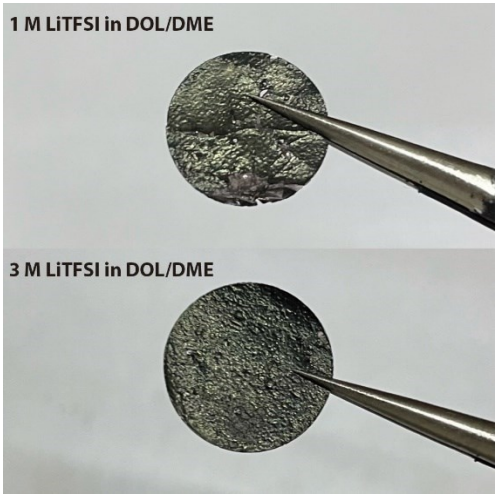

Figure S5. The image of electrodes after cycling for 1 month using 1M LiTFSI in DOL/DME and 3M LiTFSI in DOL/DME, respectively.

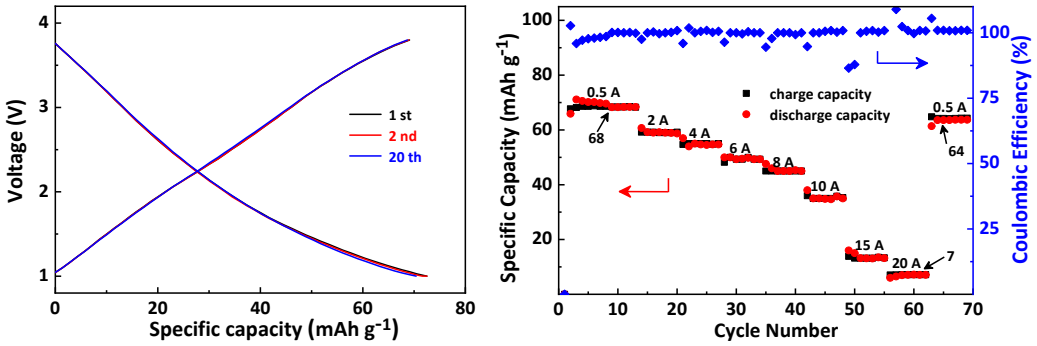

Figure S6. (a) The charge-discharge profile of KB/La133 (3:1) electrode; (b) The C-rate profile of KB/La133 (3:1) electrode.

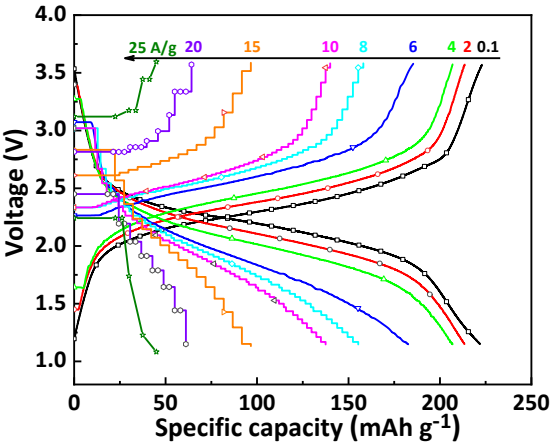

Figure S7. The charge-discharge curves of PTCDI-DAQ half cells at various current densities.

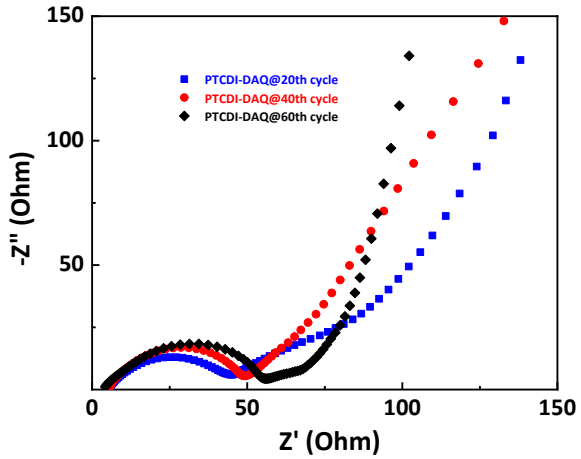

Figure S8. The EIS tests for PTCDI-DAQ cathodes after cycling.

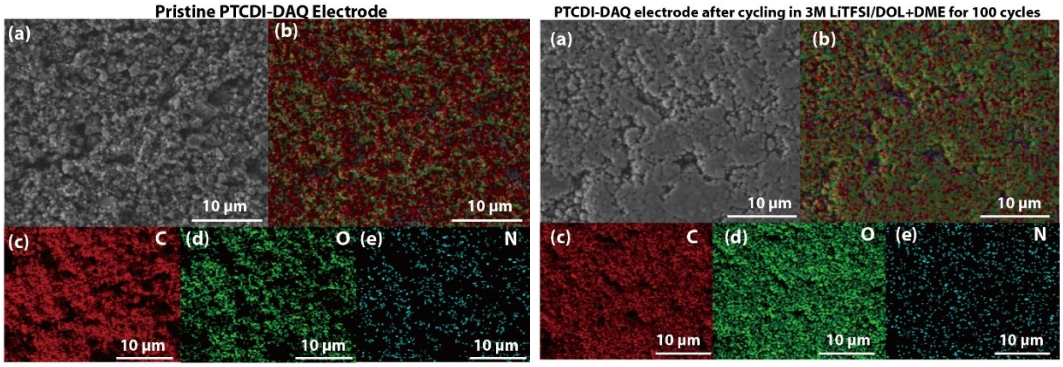

Figure S9. The (a) SEM image and (b-e) the mapping images of C, O, N elements for pristine and cycled PTCDI-DAQ electrodes.

GITT test: A constant current density of 0.5 C for 3 min and then relaxing for 30 min at open circuit (1 C corresponds to the current density of 200 mA g^{-1}) was exploited. Afterwards, the Li-ion diffusion coefficients based on the GITT results were calculated using the following equation:

$$D_{Li^+} = \frac{4}{\pi}\left(\frac{n_m V_m}{S}\right)^2\left(\frac{\Delta E_s}{\tau(dE_\tau/d\sqrt{\tau})}\right)^2 = \frac{4}{\pi}\left(\frac{V}{S}\right)^2\left(\frac{\Delta E_s}{\tau(dE_\tau/d\sqrt{\tau})}\right)^2 \approx \frac{4}{\pi\tau}(L)^2\left(\frac{\Delta E_s}{\Delta E_\tau}\right)^2$$

In this equation, $\mathbf{n_m}$ is the mole number of the active materials; $\mathbf{V_m}$ is the molar volume of active materials; **S** is the effective area of the electrode (1.13 cm^2); **τ** is the relaxation time (1800 s); **L** is the average thickness of PTCDI-DAQ electrode (58.66 μm); $\triangle\mathbf{E_s}$

is the potential change between neighboring relaxation end time; $\triangle \mathbf{E}_{\tau}$ is the potential change caused by every constant current charge/discharge process.

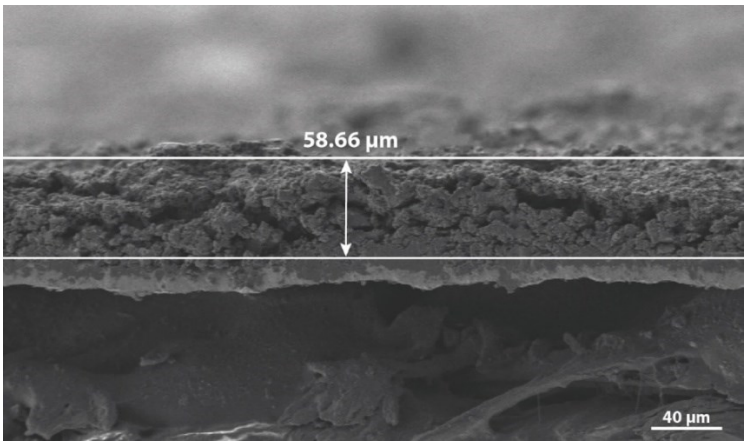

Figure S10. The thickness of PTCDI-DAQ electrode.

Table S1. Li-ion diffusion coefficient (D) of the representative cathodes in LIBs reported to date.

Cathode[a]	Technique[b]	D_{Li}^{+}[c]	Ref.
PTCCDI-DAQ	**GITT**	**1.21 x 10^{-8}**	**This work**
m-TP4OLi (O)	GITT	6.76 x 10^{-8}	[S1]
BP4OLi (O)	GITT	1.88 x 10^{-8}	[S2]
$LiMn_2O_4$ (I)	GITT	2.5 x 10^{-11}	[S3]
$Li_{1.12}[Ni_{0.5}Co_{0.2}Mn_{0.3}]_{0.89}O_2$ (I)	GITT	10^{-10}-10^{-16}	[S4]
$LiNi_{0.6}Co_{0.2}Mn_{0.2}O_2$ (I)	GITT	2.78 x 10^{-8}	[S5]
$Li(Ni_{1/3}Co_{1/3}Mn_{1/3})O_2$ (I)	GITT	3.0 x 10^{-10}	[S6]
$LiVO_3$	GITT	10^{-8}-$10^{-9.5}$	[S7]
$Li_{0.8}CoO_2$ (I)	GITT	6.4 x 10^{-4}	[S8]
$LiNi_{3/8}Co_{2/8}Mn_{3/8}O_2$ (I)	GITT	10^{-12}-10^{-16}	[S9]
$LiFePO_4$ (I)	GITT	1.8 x 10^{-15}	[S10]

[a] O=organic electrode, I=inorganic electrode; [b] GITT=galvanostatic intermittent titration technique; [c] D_{Li}^{+}= Li-ion diffusion coefficient and the unit is $cm^2\ s^{-1}$.

Electrode kinetics: The reaction kinetics of PTCDI-DAQ electrode were analyzing according to the following equations:

$$i = av^b \qquad \text{Equation 1}$$

$$\log i = b\ logv + loga \qquad \text{Equation 2}$$

In the above equations where i is the peak current of six redox peaks, v is the sweep rates, a and b are adjustable parameters. The b value could be acquired through the slope of linear fitting results in the log plot between peak current and scan rates. If b value is 0.5, the electrode is dominated by diffusion (battery behavior), whereas the process is capacity controlled (capacity behavior) when the b value is close to 1. Notably, when the b value exists between 0.5 and 1, the electrode kinetics are the hybridization of diffusion and capacitive behavior. The capacitive contribution can also be measured according to the equations below:

$$i = k_1 v + k_2 v^{\frac{1}{2}} \qquad \text{Equation 3}$$

$$\frac{i}{v^{\frac{1}{2}}} = k_1 v^{\frac{1}{2}} + k_2 \qquad \text{Equation 4}$$

k_1 and k_2 are two variables, which were only related to the potential under the condition of negligible voltage polarization change between various scan rates.

According to the variable-scan CV results, in the reduction process, the b values of peak A was 0.769, which was between 0.5 and 1, meaning that the reduction of PTCDI-DAQ was diffusion and pseudocapacitance collectively controlled. Meanwhile, the b value of peak B corresponding to the oxidation process was 0.852. The result unveiled that redox procedure of PTCDI-DAQ was dominated by synergistic battery (low test currents) and pseudocapacitance (high test currents) behaviors.

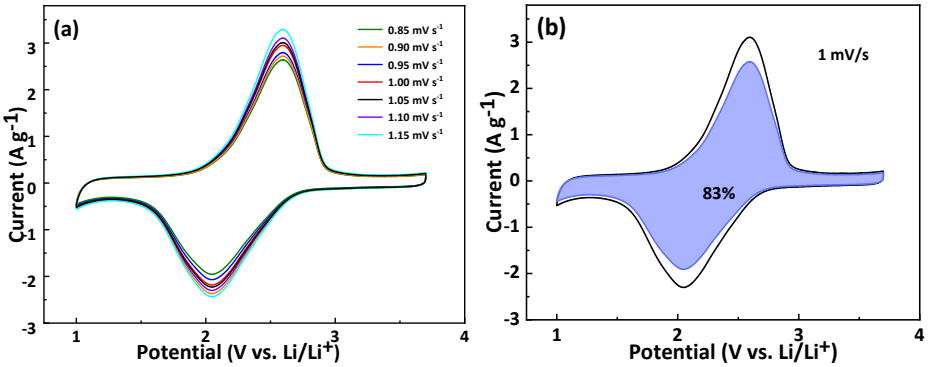

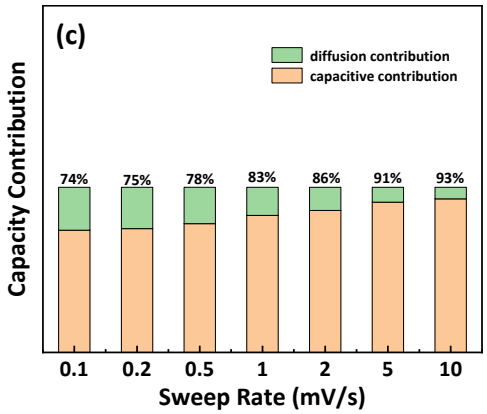

Figure S11. (a) The CV curves at the scan rates around 1 mV s-1; (b) The pseudocapacitance contribution at 1 mV s-1 for PTCDI-DAQ; (c) The pseudocapacitance contribution at various scan rates.

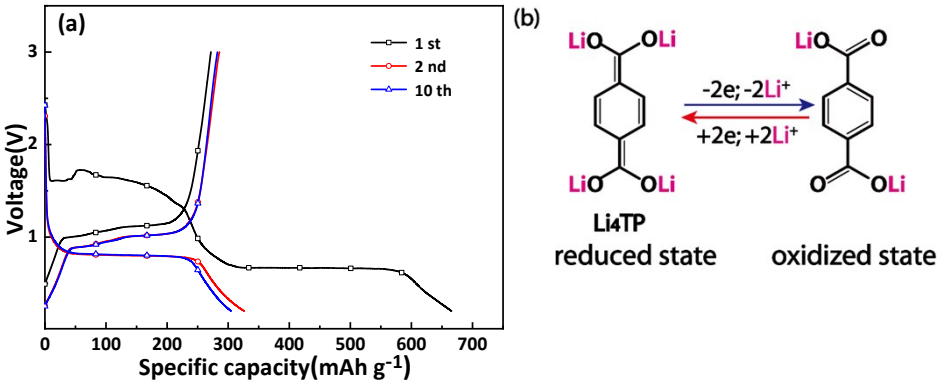

Figure S12. (a) The charge-discharge curves of H_2TP (Li_2TP) in Li-ion half cells; (b) The redox mechanism for Li_2TP in half cells.

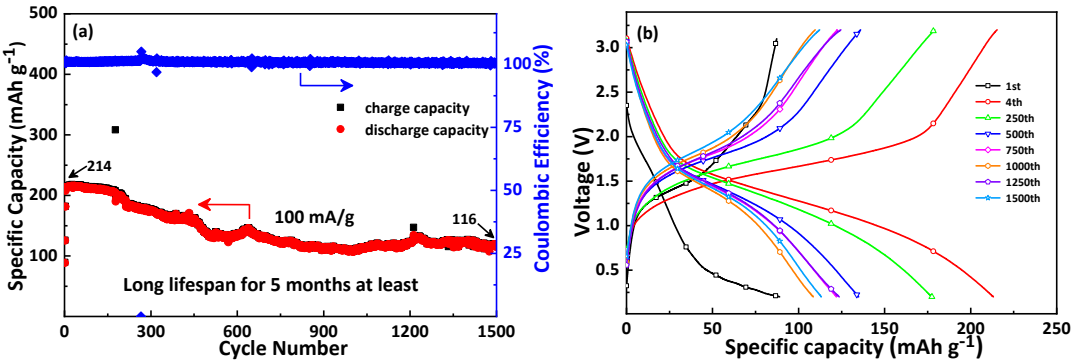

Figure S13. (a) The 1500-cycle profile and (b) The charge-discharge curves for the full cells at 100 mA g^{-1}.

References

1. Q. Yu, W. Tang, Y. Hu, J. Gao, M. Wang, S. Liu, H. Lai, L. Xu and C. Fan, *Chem. Eng. J.*, 2021, **415**, 128509-128517.
2. Q. Yu, Z. Yao, J. Shi, W. Tang, C. Wang, D. Li and C. Fan, *Org. Electron.*, 2020, **81**, 105661-105668.
3. J. Xie, K. Kohno, T. Matsumura, N. Imanishi, A. Hirano, Y. Takeda and O. Yamamoto, *Electrochim. Acta*, 2008, **54**, 376-381.
4. Y. Bai, X. Wang, X. Zhang, H. Shu, X. Yang, B. Hu, Q. Wei, H. Wu and Y. Song, *Electrochim. Acta*, 2013, **109**, 355-364.
5. A. Yaqub, Y.-J. Lee, M. J. Hwang, S. A. Pervez, U. Farooq, J.-H. Choi, D. Kim, H.-Y. Choi, S.-B. Cho and C.-H. Doh, *J. Mater. Sci.*, 2014, **49**, 7707-7714.
6. K. M. Shaju, G. V. S. Rao and B. V. R. Chowdari, *J. Electrochem. Soc.*, 2004, **151**, A1324-A1332.
7. X. M. Jian, J. P. Tu, Y. Q. Qiao, Y. Lu, X. L. Wang and C. D. Gu, *J. Power Sources*, 2013, **236**, 33-38.
8. J. Xie, N. Imanishi, T. Matsumura, A. Hirano, Y. Takeda and O. Yamamoto, *Solid State Ionics*, 2008, **179**, 362-370.
9. J. Li, X. He, R. Zhao, C. Wan, C. Jiang, D. Xia and S. Zhang, *J. Power Sources*, 2006, **158**, 524-528.
10. Y. Zhu, Y. Xu, Y. Liu, C. Luo and C. Wang, *Nanoscale*, 2013, **5**, 780-787.